

Cu/Ag(111) interface studied by surface electron energy-loss fine-structure spectroscopy

T. Tyliczszak, M. De Crescenzi,* and A. P. Hitchcock

Institute for Materials Research, McMaster University, Hamilton, Canada L8S 4M1

(Received 11 January 1988)

The structure of Cu overlayers evaporated on a Ag(111) substrate has been studied with the Cu $M_{2,3}$ surface extended energy-loss fine structure (SEELFS), recorded with an angle-resolved energy-loss spectrometer using both normal- and glancing-incidence electron beams. For coverages less than 2 monolayers (ML) an expansion of the Cu—Cu nearest-neighbor distance is observed, consistent with epitaxial growth in registry with the larger lattice size of the Ag(111) substrate. Above 2 ML the Cu—Cu distance decreases with increasing coverage until at coverages above 5 ML the Cu—Cu distance is essentially identical to that of bulk Cu. The variation of the low-energy electron diffraction pattern with Cu coverage is consistent with the SEELFS results. The Debye-Waller factors derived from the SEELFS amplitudes indicate increased thermal motion of the Cu surface atoms. The variation of the Debye-Waller factor with incidence angle for a 60-Å-thick Cu(111) film (i.e., bulk Cu) indicates anisotropic thermal motion at the surface, with motion perpendicular to the surface having a larger amplitude than that parallel to the surface.

I. INTRODUCTION

The early stages of the growth of metallic films on metals^{1,2} have been studied previously by a variety of techniques, including reflection high-energy electron diffraction (RHEED),^{2,3} valence-band electron energy-loss spectroscopy (EELS),⁴ low-energy electron diffraction (LEED),⁴ photoemission,⁵ Auger electron spectroscopy,⁶ and electron microscopy⁷ as well as x-ray photoemission spectroscopy (XPS) and Auger diffraction.⁸ A detailed understanding of the morphology of the initial stages of deposition is very important since the structure at the earliest stages nucleates further growth and thus has a profound effect on the ultimate result. Questions of interest for a particular set of substrate and overlayer elements include the following. Does the film growth proceed layer by layer or is there island formation? If epitaxial growth occurs for the lowest coverages, at what film thickness does the structure of the film adopt that of the bulk metal rather than that of the substrate? What is the structure in the accommodation region⁶ where the overlayer changes from a structure dictated by the substrate to the bulk structure of the overlayer material? Other questions which we address in this work include the magnitude of the surface thermal motion as a function of film thickness and the degree of anisotropy of the surface motion.

For the Cu/Ag(111) system studied in this work, the larger surface free energy of Cu than Ag is predicted to lead to the formation of islands of Cu on a Ag surface.⁹ However, a RHEED and electron microscopy study of this system³ has concluded that epitaxial layer-by-layer growth occurs for the first two monolayers (ML) when Cu is deposited on a room-temperature Ag(111) surface. For higher coverages or deposition at elevated temperatures of the Ag substrate, island growth occurs. In the 1–2 ML regime the RHEED measurements³ indicate an increased Cu lattice parameter. The Cu-Ag system is

particularly appropriate to study since it is one of the few metal-metal combinations for which alloy formation does not occur.^{1(c)}

The extended energy-loss fine-structure technique (EELFS) applied to surfaces (SEELFS) has been shown to be a practical, lab-based alternative to surface extended x-ray absorption fine-structure (EXAFS) studies using synchrotron radiation.^{10,11} It is ideally suited to studies of overlayers of *nd* transition metals since the $M_{2,3}$ signal falls at a convenient energy-loss region. Recently SEELFS has been used to study Cu clusters formed by island growth in the evaporation of Cu on graphite.¹² The bond-length contraction with decreasing cluster size measured by SEELFS agrees with that measured in earlier EXAFS studies.¹³ SEELFS spectra have been acquired with a variety of angle-integrated¹⁴ and angle-resolved¹⁵ EELS geometries. In this work we use a hemispherical analyzer and two electron guns in order to compare the relative surface sensitivity of normal- and glancing-incidence signals and also to investigate the capabilities of angle-resolved SEELFS to measure anisotropies of Debye-Waller factors. The anisotropy of thermal motion of surface atoms as measured by SEXAFS has been a subject of some dispute recently.^{16–20} Although the potential of SEELFS for studies of anisotropic systems has been explored experimentally and theoretically,^{20,21} this work constitutes the first report of measurements of anisotropic effects using an angle-resolved electron energy-loss spectrometer. Anisotropic effects can be probed with EELS since the momentum transfer in EELS plays the same “searchlight” role that the polarization vector plays in photoabsorption.²² In principle anisotropic structure or thermal motion effects will be larger and thus easier to observe in an angle-resolved rather than an angle-integrated experiment.

This work was accompanied by a parallel study of the same Cu/Ag(111) overlayers using extended fine Auger structure (EXFAS), the extended fine structure detected

above the Ag NVV and Cu MVV Auger peaks.^{23,24} From both SEELFS and EXFAS studies we find (1) Cu deposits epitaxially on Ag(111) with a Cu—Cu distance very similar to that of the Ag—Ag distance in the Ag substrate; (2) the commensurate registry breaks down between the third and fifth layers such that the Cu—Cu distance (in the region sampled) is essentially that of bulk Cu after 5 ML; (3) the expanded Cu—Cu distance at monolayer coverage is accompanied by increased thermal motion. In addition, the amplitude of thermal motion of the Cu atoms at the (111) surface of a 30-ML film of Cu on Ag(111) is shown to be anisotropic.

This paper is organized as follows. The apparatus and experimental techniques are presented in Sec. II A, followed in II B by details of the generation and characterization of the Cu overlayer structures by non-SEELFS techniques. The relative surface sensitivity of the normal- and glancing-incidence SEELFS is discussed in Sec. III A, while the structural information derived primarily from the glancing-incidence spectra is presented in Sec. III B. The thermal motion aspects derived from analysis of the SEELFS amplitudes are presented in III C. The main results are summarized in Sec. IV.

II. EXPERIMENT

A. Apparatus and techniques

The glancing-incidence reflection electron energy-loss spectrometer has been described previously in a brief manner in the context of the demonstration of the dipole character of SEELFS.¹⁵ Since modifications to the apparatus have been incorporated for this study, a detailed description is given. The SEELFS spectrometer (Fig. 1) is mounted on a 13-in. flange and placed in an ultrahigh-vacuum (UHV) surface analysis chamber in an inverted bell-jar configuration. The base pressure of the system is 3×10^{-10} torr, achieved by ion, Ti sublimation and cryo-cooled diffusion pumps. A retarding-grid LEED-Auger system, quadrupole mass spectrometer, and a gas-dosing system are also mounted in the chamber. Two electron

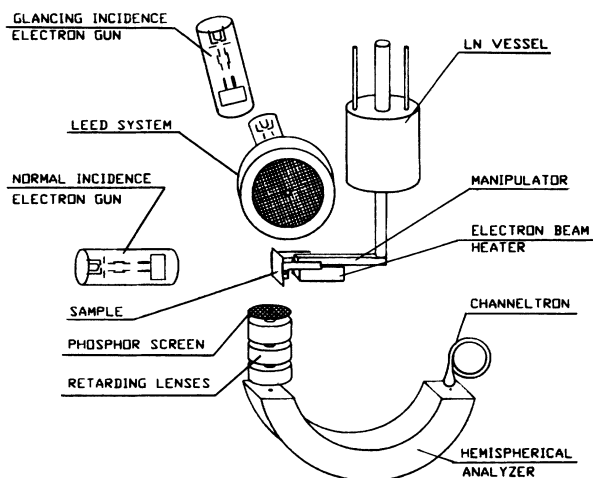


FIG. 1. Angle-resolved reflection electron energy-loss spectrometer for surface structure studies using the extended fine structure above core edges.

guns are included for SEELFS studies to allow both normal- and glancing-incidence studies. Incidence angles of 3° – 5° and exit angles of 5° – 10° were used for the glancing-incidence measurements. A second electron gun was added perpendicular to the sample-analyzer direction for normal-incidence studies. The total scattering angle is 90° in this geometry. The sample is tilted such that the exit angle of the inelastically scattered electrons is 10° – 20° relative to the surface, thus achieving a near-normal-incidence angle of 70° – 80° . The oxide cathode of the normal-incidence gun was activated in a separate high-vacuum chamber to minimize surface contamination by its outgassing. During SEELFS measurements the chamber pressure rises to $(1-5) \times 10^{-9}$ torr, with the higher values associated with residual outgassing of the normal-incidence gun.

The SEELFS spectra were acquired in first derivative [$N'(E)$] mode, using 2000 eV impact energy, incident currents of $5-15 \mu A$, analog operation of the channeltron electron detector, and lock-in detection at the first harmonic of the 800-Hz, 8-eV peak-to-peak modulation of the incident electron energy. The focusing of the electron beam was monitored with a phosphor which could be moved to the target position. The core-loss spectra shown are the average of 5 to 15 scans using a 4-sec dwell between channels and a filter time constant of 1 or 3 s. The data acquisition and energy-loss scan were controlled with an LSI-11/23 microcomputer.

B. Generation and characterization of Cu overlayers

The Cu overlayers were evaporated *in situ* at a pressure of $(1-2) \times 10^{-9}$ torr. Prior to evaporation the Ag(111) crystal was cleaned by Ar-ion bombardment until Cu or any impurity could not be detected by Auger. It was then annealed ($300^\circ C$, 5 min) until a high-quality Ag(111) LEED pattern was obtained. The average Cu film thickness was monitored during evaporation by a quartz microbalance thickness monitor, the head of which was mounted close to the Ag(111) substrate, at the same radial distance from the Cu evaporation source. The film thicknesses quoted in this paper are those derived from the quartz microbalance. The relative thickness scales are estimated to be accurate to a few percent and the absolute coverage to be accurate within 50%. The greater uncertainty in the absolute film thickness takes into account possible systematic errors such as angular anisotropy of the Cu evaporation (the sample was oriented at 45° while the quartz crystal was oriented at 90° to the surface from which the Cu was evaporated). The evaporation source consisted of pieces of oxygen-free, high-conductivity Cu in a tungsten wire basket. Apart from an opening the size of the Ag(111) substrate, the evaporation source was enclosed by a stainless-steel shield to protect other parts of the apparatus. The films were deposited onto a room-temperature Ag(111) surface with a small off-normal incidence angle (80° relative to the surface plane), at a rate of $2-5 \text{ \AA}/\text{min}$. The uniformity of the evaporation was confirmed by observing that the Auger and LEED signals were essentially identical over the complete Ag surface. This is particularly important for

the glancing angle geometry, where the electron beam extends over 15 mm of the surface.

The LEED pattern remained sharp and did not change its position for all coverages up to 4 Å, which corresponds to approximately 2 ML based on a sticking coefficient of unity and density-packing considerations. For Cu coverages between 4 and 10 Å (2–5 ML) the pattern became fuzzy but never disappeared. Above 10 Å (5 ML) the LEED pattern became sharp again, exhibiting the pattern of Cu(111). The scattered electron signal on the phosphor screen mounted above the energy-loss analyzer (see Fig. 1) exhibited circles of diffraction streaks [medium-energy electron diffraction (MEED)] for clean Ag(111). These became progressively fuzzier with Cu deposition and did not reform for coverages above 10 Å. We interpret this to indicate an appreciable roughness of the Cu surface on a scale that affects the glancing-incidence MEED but not the normal-incidence LEED diffraction.

Auger spectra of the clean Ag(111) and at various Cu coverages are shown in Fig. 2. The Auger spectrum recorded after a 2–4-h SEELFS acquisition was indistinguishable from that recorded just after preparation of the overlayer. In principle, if layer-by-layer growth occurs, a plot of the Auger intensity versus coverage (as measured by the quartz microbalance) should show slope changes

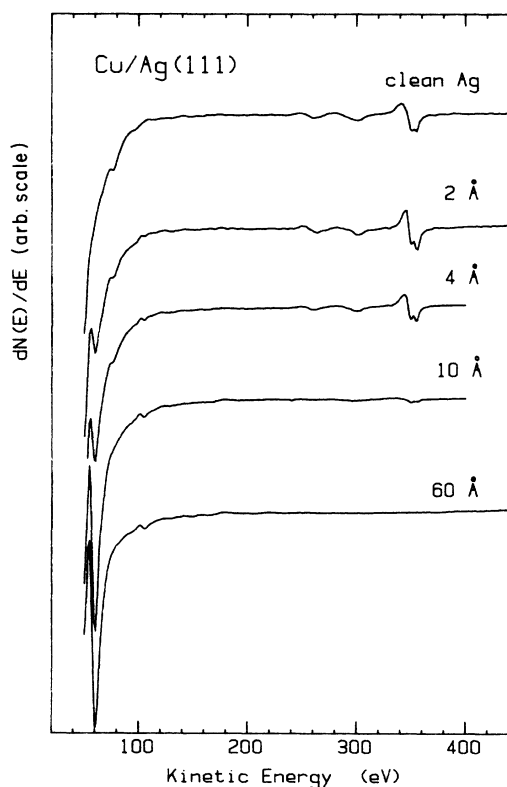


FIG. 2. First derivative Auger spectra recorded with a retarding-grid system. The figures to the right of each curve indicate the nominal coverage in Å of Cu deposited on a clean Ag(111) substrate by *in situ* evaporation, as measured by a quartz microbalance thickness monitor. The number of monolayers is approximately half the thickness in Å.

when successive layers are completed.^{1,25} However, such breaks are not always detectable⁴ and in any case, the Auger spectra were measured at too coarse a coverage mesh to search for the expected breaks.

III. RESULTS

A. Surface sensitivity

Figure 3 presents the normal incidence, first derivative (N') energy-loss spectra of clean Ag(111) and the same surface covered with Cu films of 2, 4, 10, and 60 Å average thickness (corresponding to coverages of 1, 2, 5, and 30 ML, respectively). The energy-loss scale for each spectrum was established precisely by a measurement of the elastic peak prior to and following acquisition of the core-loss spectrum. The normal-incidence energy-loss spectra are dominated by the Ag $N_{2,3}$ structure at coverages below 4 Å while the Cu $M_{2,3}$ signal dominates at coverages of 10 Å and larger. The Cu $M_{2,3}$ edge jump overlaps the last large structure in the Ag $N_{2,3}$ near-edge signal so that the exact onset of the Cu $M_{2,3}$ signal is difficult to detect. The Fourier transforms (Fig. 4) of the Cu $M_{2,3}$ SEELF signal in these spectra reflect the Cu environment for the 10- and 60-Å coverages but are severely distorted by the underlying Ag $N_{2,3}$ signal for coverages of 4 Å and below, to the point where the transform of the 2-Å spectrum contains only "noise" (components at all radial distances, arising from the Ag $N_{2,3}$ signal, for

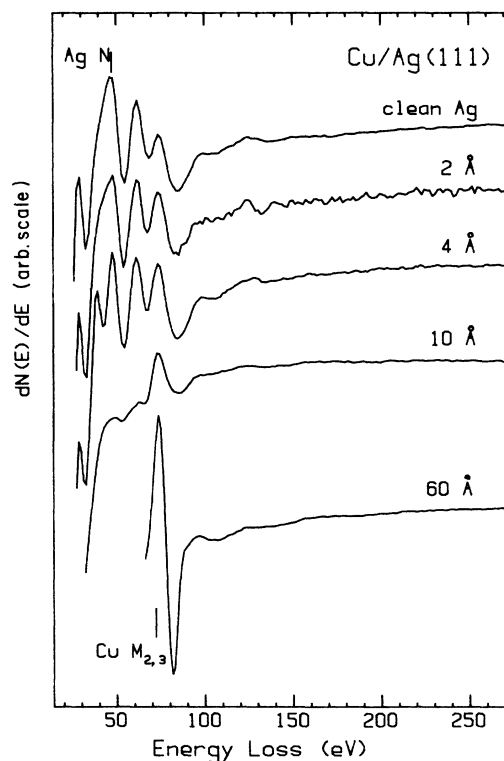


FIG. 3. First derivative reflection electron energy-loss spectra [$N'(E)$ EELFS] of clean and Cu-covered Ag(111) recorded with 2000 eV impact energy, a 90° angle between beam and analyzer, and a 10°–20° exit angle (normal-incidence geometry).

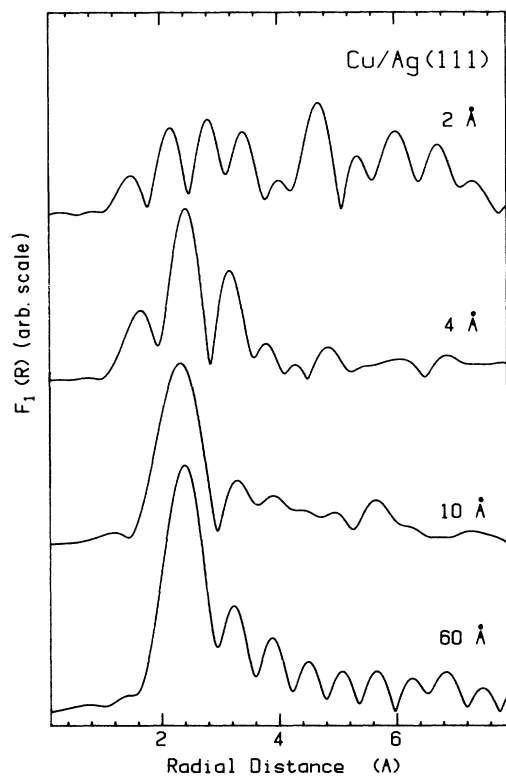


FIG. 4. Magnitudes of the Fourier transforms of the k^{-1} -weighted extended fine structure from the Cu $M_{2,3}$ normal-incidence EELFS. The signal for 2 Å of Cu on Ag(111) is dominated by the Ag $N_{2,3}$ EELFS (see Fig. 3) which is grossly distorted from that expected for the Fourier transform of Ag EELFS because the origin of the k scale is set to the Cu $M_{2,3}$ rather than the Ag $N_{2,3}$ edge.

which the k scale is defined incorrectly). At 4 Å and above a reasonable signal is observed, although that at 4 Å is heavily contaminated with the underlying Ag $N_{2,3}$ noise.

In contrast to the normal-incidence spectra, the glancing-incidence $N'(E)$ spectra for the corresponding sequence of Cu overlayers on Ag (Fig. 5) show a much greater surface sensitivity such that the Cu $M_{2,3}$ signal clearly dominates the underlying Ag $N_{2,3}$ signal, even at 2 Å (1 ML). The background in the glancing-incidence geometry has a steeper curvature than for normal incidence. It is also less uniform from spectrum to spectrum. We attribute both effects to background contributions from the wings of the incident electron beam, which enter the energy-loss analyzer directly and are not completely filtered from the inelastic signal of interest. There is essentially no background of this type in the spectra recorded with the normal-incidence geometry. The glancing-incidence background varies with the analyzed energy. It is also a sensitive function of the electron beam and sample positions.

Comparison of Figs. 3 and 5 clearly shows that the surface sensitivity at glancing incidence is *much* greater than that at normal incidence. This has been demonstrated in previous studies of the angular variation of valence-band energy-loss signal by several groups.^{26,27} In one sense this

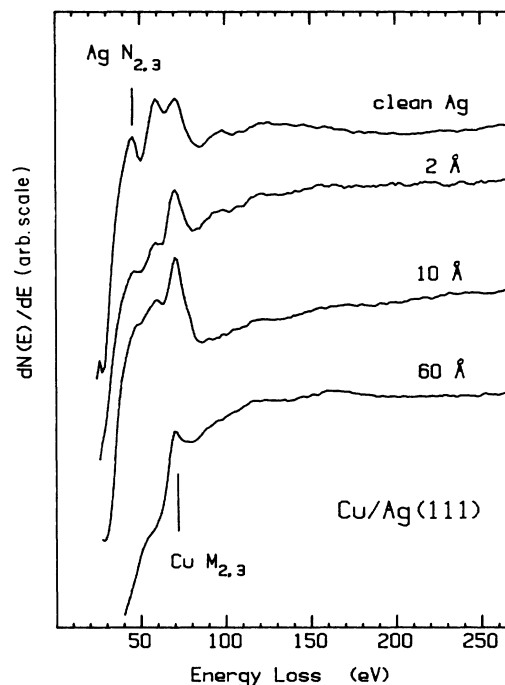


FIG. 5. $N'(E)$ EELFS of clean and Cu-covered Ag(111) recorded with 2000 eV impact energy, a 170° angle between beam and analyzer and a 6° exit angle (glancing-incidence geometry). The indicated Cu coverage is the evaporated film thickness as measured by the quartz microbalance and is approximately twice the coverage in ML.

is as expected on account of the much shallower penetration of the electron beam in the glancing geometry. However, it is noteworthy that the exit angle of our normal-incidence geometry is almost as shallow as that in the glancing-incidence geometry. It appears that a shallow *incidence* angle is much more effective than a small exit angle in enhancing the surface sensitivity of SEELFS. The very small Ag $N_{2,3}$ signal in the glancing-incidence spectra of the Cu films thinner than 6 Å supports the occurrence of layer-by-layer growth in the initial stages since a considerably stronger Ag $N_{2,3}$ signal would be observed if large regions of Ag were exposed. The residual Ag $N_{2,3}$ signal in the Auger and SEELFS spectra of 10-Å films and greater (Figs. 2, 3, and 5) probably arises from the regions between the Cu islands³ where the Cu coverage is only 1–2 ML.

B. Structure of Cu overlayers on Ag(111)

The extended fine structure was isolated from the SEELFS spectra shown in Figs. 3 and 5 using a two-section cubic spline background function in each case. The Cu $M_{2,3}$ ionization threshold (74 eV) was used as the origin of the wave-number scale for the SEELFS signal. The glancing-incidence spectra, which are dominated by the Cu $M_{2,3}$ signal even at 1 ML coverage, give good structural information down to the lowest coverages studied. (Although the Cu $M_{2,3}$ signal could be detected at submonolayer coverage, we were interested in Cu—Cu

distances and wanted to work in a coverage regime where the contributions of Ag backscattering to the Cu $M_{2,3}$ SEELFS could be neglected.) The extended fine structure extracted from selected glancing-incidence SEELFS are presented in Fig. 6. The glancing-incidence spectra recorded in the $N'(E)$ mode were integrated prior to analysis in order to reduce distortion of the higher R components of the radial distribution.²⁸ The Fourier transform (FT) magnitudes of the SEELFS at 2-, 3-, 6-, 10-, and 60-Å coverages are shown in Fig. 7. At all coverages studied the nearest-neighbor (NN) signal dominates. There is a dramatic shift to higher R values in the position of the NN signal in the transform below 10 Å. The changed NN distance can also be observed in the untransformed data (Fig. 5), in the form of a compression of the oscillatory signal at low coverages, which results in a reversal of the phase around 6 \AA^{-1} between the data for 3- and 10-Å coverages. For coverages above 10 Å no significant further changes occurred in the SEELFS or its FT, indicating that the outer 1–2 layers sampled have identical structure for all Cu films thicker than 5 ML on a Ag(111) substrate. Quantitative analysis (see below) of the Cu $M_{2,3}$ SEELFS indicates essentially a bulklike Cu—Cu nearest-neighbor distance at the surface for coverages of 10 Å and larger.

The higher shells do not seem as well developed in the glancing-incidence SEELFS of the 60-Å-thick film as compared with the $M_{2,3}$ SEELFS of bulk Cu.^{10,28} However, the normal-incidence SEELFS of the 60-Å film

(Figs. 3 and 4) shows greater higher shell signal, approximately like that observed in the EELFS of bulk Cu recorded with angle-integrated techniques (Refs. 12 and 28–30—see also Fig. 8). This suggests that the reduced higher shell signal at glancing incidence may reflect poor longer-range ordering of the topmost Cu layers, as is also suggested by the differences in the MEED and LEED for the 60-Å film. Attempts to anneal the 60-Å-thick film to improve the ordering were frustrated by a rapid increase in the Ag signals in the Auger and SEELFS, indicating either Ag segregation to the surface or growth of larger Cu islands, thus exposing more of the Ag substrate.

We interpret the SEELFS results in terms of the formation of epitaxial layers of Cu on the Ag(111) substrate, which are commensurate with the Ag lattice below 2 ML and convert to a Cu bulklike overlayer above 2 ML coverage. The preservation of the Ag(111) LEED pattern with no changes in the spot spacing at a fixed voltage up to 4 Å (2 ML) coverage, supports our interpretation of the commensurate structure at the lowest Cu coverages. The variation in the LEED patterns at higher coverages is also consistent with the SEELFS results and our interpretation of the development of the overlayer structure.

Our results agree with those of the RHEED and electron microscopy studies^{3,7} which indicate that layer-by-layer epitaxial growth occurs in the initial stages of the deposition of Cu on room-temperature Ag. At higher coverages, the microscopy^{3,7} shows that the majority of

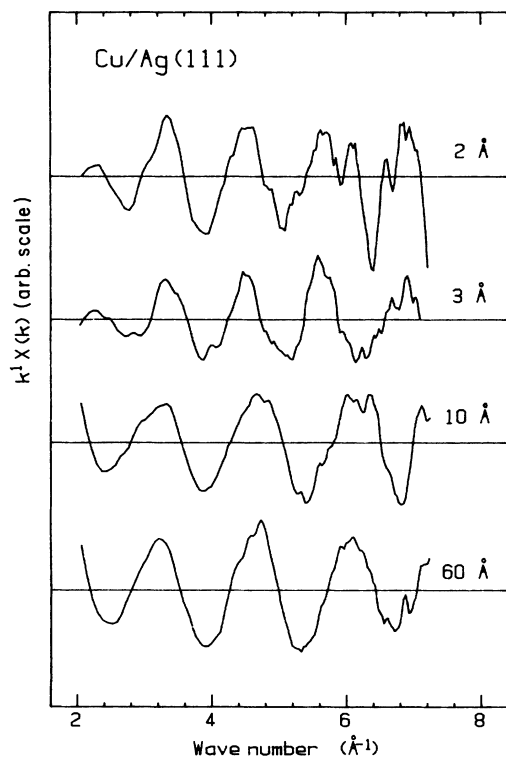


FIG. 6. k^1 -weighted EELFS [$X(k)$] derived with a two-section cubic spline background subtraction from the integrated glancing-incidence spectra recorded from Cu films of the indicated thickness.

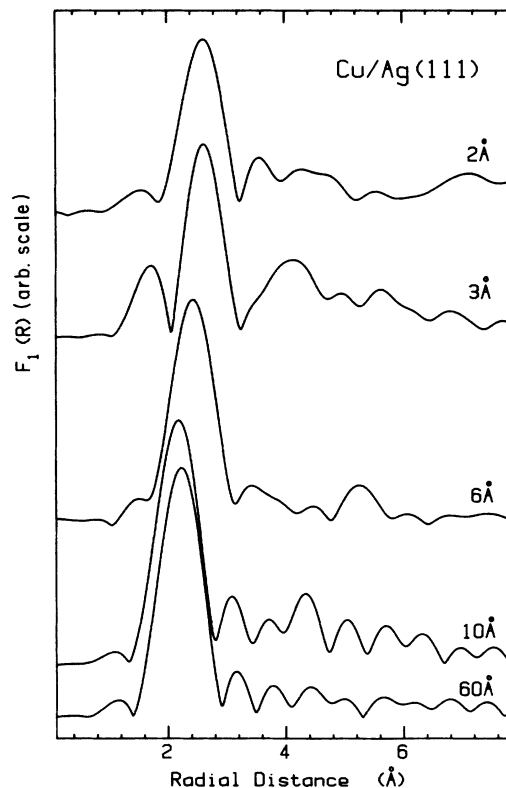


FIG. 7. Magnitudes of the Fourier transforms of the $k^1 X(k)$ $M_{2,3}$ glancing-incidence EELFS of 2-, 3-, 6-, 10-, and 60-Å-thick films. Note the shift to larger R and the broadening of the nearest-neighbor peak in the data from the thinner layers.

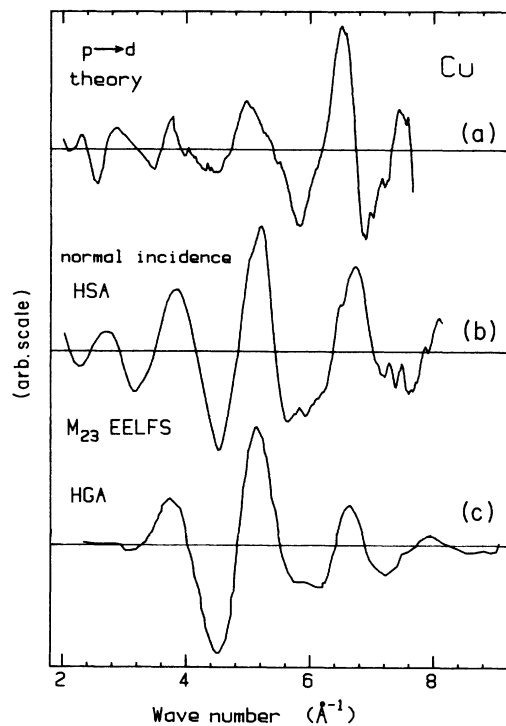


FIG. 8. Comparison of (a) the $p \rightarrow d$ continuum shape from the L_2 band-structure calculations of Albers *et al.* (Ref. 34); (b) the Cu $M_{2,3}$ EELFS of 60 Å (30 ML) of Cu on Ag(111), recorded in normal-incidence geometry with an angle-resolved hemispherical analyzer (HSA); and (c) the angle-integrated EELFS of polycrystalline Cu, recorded by Idzerda *et al.* (Ref. 14) with a retarding hemispherical grid analyzer (HGA).

the surface is covered with islands of similar height.³ In this regime SEELFS probably cannot distinguish layer-by-layer or island growth, since the technique is only sensitive to local structure. Bruce and Jaeger⁷ observed that the interference fringes associated with the mismatch of the Cu and Ag crystal spacings developed very rapidly with increasing thickness of the Cu deposited on a Ag film such that the mismatch was accommodated in a very few layers. Similarly, Horng and Vook³ found that the lattice spacing derived from RHEED is increased (by 0.04 Å) in Cu films thinner than 3 Å but that the lattice spacing of bulk Cu is observed for films thicker than 4 Å. Thus all experimental results to date indicate an initial layer-by-layer growth for Cu deposition on ambient temperature Ag, in contradiction to thermodynamic expectations.³ The Cu/Ag(111) and Ag/Cu(111) systems appear to be similar since layer-by-layer growth with commensurate epitaxy in the first layers has been deduced from valence-band measurements of Ag films on Cu(001).²⁵ In the Ag/Cu(001) system the band structure of the Ag film was found to be two dimensional for a single layer but to have converted to a bulklike three-dimensional band structure after five layers.

The increased nearest-neighbor distance observed in the lowest coverages could be interpreted as arising from contributions from backscattering by the Ag substrate. However, we argue that backscattering from Ag makes

negligible contribution to the SEELFS signal in our measurements. First, the Cu—Ag bond length should be between that of bulk Cu (2.55 Å) and bulk Ag (2.89 Å), whereas the SEELFS of the thinnest films (Table I) suggests a nearest-neighbor distance very similar to that of Ag—Ag. Second, the results from 2–4-Å coverages are all very similar, whereas a shift to lower R should be observed if there was a decreasing contribution from Ag backscattering as the Cu overlayer thickens. Third, in the case of a single, perfect, commensurate monolayer with isotropic sampling of the NN radial distances, the Cu backscattering signal would be twice as strong as that from Ag, based on numbers of atoms. Fourth, the Ag backscattering amplitude has a very characteristic minimum around 6 Å⁻¹ (Ref. 31) which should be detected in our first shell amplitude function if there is appreciable backscattering from Ag. Finally, the variation of the SEELFS amplitudes with incident angle indicates that the glancing-incidence spectrum is preferentially sensitive to in-plane distances on account of the orientation of the momentum transfer predominantly parallel to the surface (see Sec. III C). All of these points suggest that the Ag backscattering signal is at most a minor contribution and that the observed Cu $M_{2,3}$ SEELFS reflects predominantly the expanded Cu—Cu distance of the Cu overlayer which is in registry with the underlying Ag substrate.

Quantitative results for the nearest-neighbor distance require correction for the effects of absorber and backscatter phase shifts. As observed in the analysis of the $M_{2,3}$ extended fine structure of other 3d transition metals,^{10,28} the application of calculated phases—either $L_{2,3}$,³¹ or $M_{2,3}$ (Ref. 32)—to the 60-Å-thick film results in a predicted NN distance that is 0.2 Å shorter than that of bulk Cu. Although there has been much discussion of the possibility that nondipole contributions are the cause of this error, this has been ruled out on several grounds. First, an identical error is observed in the $M_{2,3}$ EXFAS of Co (i.e., as measured by synchrotron radiation³³). Second, there is very good agreement between normal-incidence, angle-resolved SEELFS (present work) and that recorded with a retarding-grid analyzer which integrates over a much larger range of momentum transfer.¹⁴ This comparison is made in Fig. 8, which also plots the L_2 extended fine structure of Cu calculated by Albers *et al.*³⁴ using band-structure techniques. The main features of the calculated L_2 and experimental $M_{2,3}$ spectra are aligned, with particularly good agreement of both

TABLE I. Nearest-neighbor distances derived from glancing-incidence SEELFS of Cu overlayers on Ag(111).

Cu film thickness (Å)	R (Å)	
	Normal	Phase model (60-Å film) = Glancing
2	3.03	2.95
3	3.03	2.95
6	2.91	2.83
10	2.60	2.53
60	2.64	2.56

intensity and position between the normal-incidence, angle-resolved and the angle-integrated $M_{2,3}$ SEELFS. This provides further support of the dominantly dipole character of $M_{2,3}$ SEELFS (Refs. 10, 11, and 15) and complements our earlier comparison of glancing-incidence and angle-integrated, normal-incidence SEELFS (taken using a cylindrical mirror analyzer) of nickel.¹⁵ However, the phase-shift problem is revealed in Fig. 8 through the dephasing that occurs between the Cu $M_{2,3}$ SEELFS and the L_2 theory, over the whole k range plotted. Several origins for this phase-shift problem have been discussed recently. One suggestion is that the problem is associated with the inapplicability of the $Z+1$ approximation³⁵ used to treat the core hole. This is not the case since an $M_{2,3}$ phase shift calculated without the $Z+1$ approximation³² gave a similar error in the first shell distance.²⁸ A second suggestion³⁶ that the additional phase shift arises from $p \rightarrow s$ contributions (neglected in the normal EXFAS treatment of p -shell ionization) was recently refuted³⁷ with the aid of accurate *ab initio* calculations which showed that the $p \rightarrow d$ ionization channel is three to six times more intense than the $p \rightarrow s$ channel for all 3d transition metals.

Although the exact origin of the additional phase shift for $M_{2,3}$ extended fine structure remains to be clarified, experimentally derived phase shifts can provide quantitative structural information, assuming, as usual, that the phase shift does not change from model to sample. In this case we require only that the Cu-Cu phase shift is independent of the thickness of the Cu overlayer. Thus we have assumed that the Cu—Cu distance in the surface region of the 60-Å-thick sample corresponds to that of bulk Cu (2.56 Å) and we have used the 60-Å data to derive experimental Cu $M_{2,3}$ phase shifts for use as standards for the other measurements. A possible limitation here is that the Cu-Cu spacing in this region may differ from that of bulk Cu due to surface tension effects. Indeed LEED studies suggest that there is a 4% contraction of the first and second layer spacing relative to that of the bulk for the Cu(111) surface.³⁸

Table I summarizes the distances derived from the glancing-incidence data using both the normal- and glancing-incidence spectra of the 60-Å film as the phase standard. The expansion of the Cu—Cu NN distance in the 2- and 3-Å films that is shown qualitatively in Fig. 7 is verified quantitatively. The Cu—Cu distance in the monolayer regime is 0.39(6) Å larger than that of bulk Cu, in good agreement with the 0.33-Å difference between the NN distances of bulk Cu and Ag. However, the increase in the Cu-Cu spacing deduced from SEELFS is considerably larger than the 0.04-Å increase in the Cu lattice parameter observed by the RHEED measurements of Horng and Vook³ on the same surface. The difference here may be related to differences in the depth sensitivity and/or the directions in which RHEED and SEELFS probe.

For each film thickness the NN distance derived using the normal-incidence phase is systematically 0.08 Å larger than that derived with the glancing-incidence phase model. This can be attributed to the difference in the directional sensitivities of the two scattering

geometries. As explained in Sec. III C, the glancing-incidence geometry samples predominantly in the surface plane (where the Cu—Cu distance in the 60-Å film has the bulk value) while the normal-incidence geometry samples preferentially along the surface normal [where LEED (Ref. 38) indicates a 4% or 0.10-Å contraction]. The larger NN distances systematically observed using the normal-incidence data of the 60-Å film as the model can then be attributed to the use of the incorrect Cu-Cu NN spacing (that of the bulk rather than the contracted NN spacing) when extracting the phase model.

In this analysis the k -scale origin parameter (E_0) was adjusted according to a standard technique³⁹ in order to achieve a zero intercept to the difference of the phase functions of the model and unknown. For a given phase model the E_0 values varied by less than 2 eV. This extent of E_0 variation has an insignificant effect on the derived Cu—Cu distance (<0.02 Å) as was confirmed by carrying out the analysis with a fixed E_0 .

Very little variation of the Cu—Cu NN distance is observed in the analysis of the normal-incidence data for the 4-, 10-, and 60-Å thick Cu films. This is consistent with the negligible shift in the NN peak position observed in Fig. 4. The insensitivity of this scattering geometry to the structural changes observed with the glancing-incidence geometry is consistent with a preferential sampling of the film perpendicular to the surface, along with averaging over a larger number of layers owing to the greater sampling depth in the normal- than the glancing-incidence geometry. Some increase in the NN spacing is expected in the 4-Å film; however, this is probably masked by the distortion caused by the underlying Ag $N_{2,3}$ extended fine-structure signal.

C. Thickness and angle variation of Debye-Waller factors

The NN backscattering amplitude functions were derived from back Fourier transforms of the filtered first shell SEELFS. The amplitude curves extracted from the Fourier-filtered first shell signal in the glancing-incidence SEELFS ($T=25^\circ\text{C}$) of the 2-, 3-, 6-, 10-, and 60-Å films are compared in Fig. 9. The amplitude curves for the

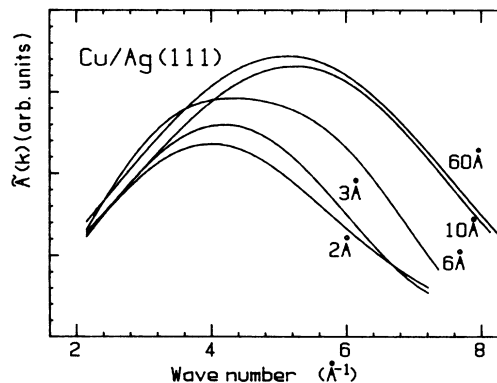


FIG. 9. Amplitude functions derived from the Fourier-filtered EELFS recorded in glancing-incidence geometry at room temperature on the indicated thicknesses of Cu overlayers on Ag(111). The reverse transform was taken of the data between 1.2 and 3.6 \AA^{-1} weighted by a Hanning window.

60-Å film recorded with normal incidence at -130 and 25°C are compared to the amplitude curve from the glancing-incidence spectrum of the 60-Å film at 25°C in Fig. 10. The Debye-Waller factors extracted from the normal- and glancing-incidence Cu $M_{2,3}$ SEELFS at all coverages studied are summarized in Table II. These relative values were derived using standard EXFAS procedures^{39,40} which assume Gaussian distance distributions. Idzerda *et al.*⁴¹ have recently discussed in some detail the procedures required to derive accurate Debye-Waller factors from SEELFS measurements, in their case in the context of a study of the structure of Ti films deposited on Si(111).

All the glancing-incidence spectra were recorded at room temperature and thus the shift to lower k in the amplitude maximum below 10 \AA^{-1} (Fig. 9) is a result of the larger-amplitude thermal motion associated with the more weakly bonded, stretched Cu—Cu distance in the commensurate epitaxial overlayer. The 2-, 3-, and 6-Å curves indicate a continuous rather than an abrupt transfer from a monolayer structure commensurate with the Ag(111) surface to a bulk-Cu-like structure of the Cu overlayer. The negligible difference between the Debye-Waller factors derived from the glancing-incidence SEELFS of the 10- and 60-Å-thick films indicates that the surface regions of these Cu films do not sense the Ag substrate. Thus the intrinsic character of the surface of bulk Cu metal has been achieved by 5 ML. The dramatic rise in the thermal motion (Debye-Waller factor) for films less than 10 \AA thick is consistent with a loosely bound, stretched system. Based on the measurements of bulk Cu,^{40,42,43} this corresponds to a mean-square relative displacement similar to that of bulk Cu around $600\text{--}700^\circ\text{C}$. In the normal-incidence SEELFS, the shift of the amplitude maximum to higher k with increased temperature is exactly that expected for reduced vibrational motion at lower temperature. The variation of mean-square relative displacement (σ^2 , MSRSD) of the 60-Å film between -130 and 25°C (room temperature) is very close to that reported from K -shell EXFAS measurements of bulk Cu, where an increase of $3.2 \times 10^{-3} \text{ \AA}^2$ between 150 and 295 K is observed.^{40,42,43} This further supports our interpretation that the average structure in the outer 3–5 layers of the 60-Å Cu film sampled by the normal incidence SEELFS is essentially identical to bulk Cu. The variation of the MSRSD with temperature that we observe is also similar to the $4.7 \times 10^{-3} \text{ \AA}^2$ change between 77 and 300 K for Cu deposited on Co.¹⁶

One of the goals of this research was to see if angle-resolved SEELFS recorded in glancing- and normal-

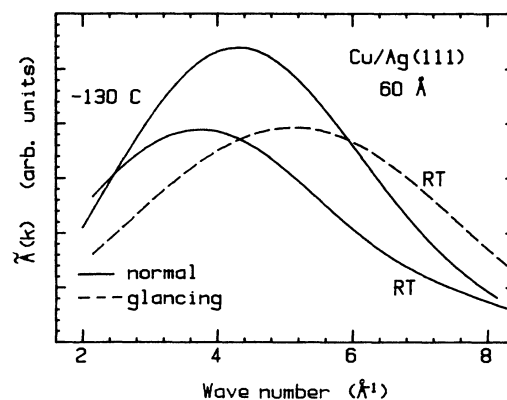


FIG. 10. Amplitude functions derived from the SEELFS recorded in normal-incidence geometry on a 60-Å-thick Cu overlayer at -130 and 25°C . The amplitude function derived from the glancing-incidence spectrum of the same film recorded at 25°C is also plotted. The difference between the glancing- and normal-incidence SEELFS amplitudes arises from the anisotropy of surface vibrational motion (see text).

incidence geometries could provide information about the directional distribution of the thermal motion of surface atoms. Comparison of our glancing- and normal-incidence amplitude curves (Fig. 10) reveals a dramatic shift to lower k of the amplitude maximum in the normal-incidence SEELFS of the 60-Å film at RT, relative to the same sample recorded in glancing geometry. This shift is *not* in the direction expected from the difference in sampling depths of the two scattering geometries. The general expectation (e.g., as indicated by LEED results⁴⁴) is that the thermal motion in the near surface is larger than that of the bulk. Based on the clearly greater surface sensitivity of the glancing-incidence geometry, this would lead to a larger Debye-Waller term in the glancing- rather than the normal-incidence geometry, contrary to our observation.

We interpret the change in Debye-Waller factor with scattering geometry in terms of a strong *directional* variation of the energy-loss signal with the incidence angle of the electron beam. Our results indicate a larger thermal motion in the direction sampled preferentially by the normal-incidence scattering geometry. The similarity of angle-resolved and angle-integrated results (Fig. 8) indicates that the SEELFS signal is dominated by events consisting of a zero-degree inelastic combined with an elastic scattering of the appropriate angle. This has been the

TABLE II. Debye-Waller factors from SEELFS of Cu/Ag(111). All samples were measured at 25°C .

Geometry	Sample (Cu thickness)	Reference	σ^2 (10^{-3} \AA^2)
Normal	60 Å	60 Å, normal, -130°C	2.5(5)
Normal	60 Å	60 Å, glancing, 25°C	12.0(1)
Glancing	2 Å	60 Å, glancing, 25°C	13.8(5)
Glancing	3 Å	60 Å, glancing, 25°C	14.1(5)
Glancing	6 Å	60 Å, glancing, 25°C	8.3(5)
Glancing	10 Å	60 Å, glancing, 25°C	-0.2(5)

conclusion of all SEELFS studies to date.^{10,11,14,15,28,45,46} Thus the momentum transfer is in the direction of the incident electron beam for loss-diffraction (LD) events and in the direction of the outgoing electron beam for diffraction-loss (DL) events.^{47,48} For our glancing-incidence geometry this implies that the momentum transfer is primarily in the plane of the surface (i.e., the glancing-incidence geometry is most sensitive to motion parallel to the surface). For the normal-incidence geometry, the DL processes also sample the motion parallel to the surface but the LD processes probe the motion perpendicular to the surface. With an impact energy large relative to the energy loss, one expects roughly equal contributions from LD and DL processes.^{45,46} Based on these arguments, the larger Debye-Waller factor (i.e., more rapid damping with k) in the normal-incidence geometry indicates that the amplitude of thermal motion is larger perpendicular to the surface than that in the surface plane. This result for Cu(111) agrees with that for the Ni(100) surface derived from a similar comparison of glancing- and normal-incidence SEELFS.⁴⁸ The surface anisotropy at the Cu(111) surface is such that the difference in mean-square relative displacement between the directions sampled by the two geometries is almost as great as that between bulk Cu and that in the commensurate first layer of Cu on the Ag(111) surface (Table II). Greatly increased thermal motion of the Cu surface atoms perpendicular to the surface may be associated with a reduced melting temperature of the surface layer of Cu, as has been suggested recently.⁴⁹

According to our results, the directional anisotropy of thermal motion at the Cu surface is in the same sense as that for Cu on Co (Ref. 16) and oxygen on Cu (Ref. 18) as derived from SEXAFS, but is in the opposite sense to that for atomic Cl in a $c(2 \times 2)$ overlayer on Cu(100) (Ref. 19) and N on Ni(100) (Ref. 20). In the latter two cases, the SEXAFS results indicate that motion parallel is larger than motion perpendicular to the surface. It is particularly noteworthy that for the 60-Å-thick film the

difference between the parallel and perpendicular motion indicated by our results cannot be attributed simply to differences in the chemical-bond strengths, as is likely the case in all previous extended fine-structure measurements^{16,18-20} of the anisotropy of surface vibration.

IV. SUMMARY

SEELFS employing angle-resolved electron energy analysis with glancing- and normal-incidence-electron beams has been used to study the structure of Cu overlayers on a Ag(111) surface. Epitaxial growth in registry with the Ag(111) substrate is observed for the first 2 ML while a transition to the interatomic spacing of bulk Cu(111) occurs between 6 and 10 Å, corresponding to completion of the third to fifth layers. Enhanced thermal motion in the commensurate epitaxial layer is observed. Between the monolayer and > 5 ML regimes, the variation of the NN distance and thermal motion is found to be smooth rather than discontinuous. Comparison of the amplitude functions of the normal- and glancing-incidence room-temperature spectra of the 60-Å Cu(111) film on Ag(111) indicates that the motion perpendicular to the surface has greater amplitude than that parallel to the surface. Finally, the similarity of the normal-incidence SEELFS of the 60-Å Cu(111) film as compared to that from various angle-integrated measurements provides further support for the electric-dipole origin of $M_{2,3}$ SEELFS.

ACKNOWLEDGMENTS

We thank Dr. J. Stöhr for providing the Ag(111) crystal used in this experiment, and S. A. C. Clark for assistance with the acquisition and analysis programs. Financial support for the research was provided by the Natural Science and Engineering Research Council (NSERC) (Canada) and by the Imperial Oil Co. The support of an International Scientific exchange grant for Dr. De Crescenzi is gratefully acknowledged.

*Permanent address: Dipartimento di Fisica, Università di Roma II, "Tor Vergata," 00173, Rome, Italy.

¹(a) *Epitaxial Growth*, edited by J. W. Matthews (Academic, New York, 1975); (b) G. E. Rhead, *Contemp. Phys.* **24**, 535 (1983); (c) E. Bauer, in *Chemical Physics of Solid Surfaces*, edited by D. A. King and D. P. Woodruff (Elsevier, Amsterdam, 1984), Vol. 3B.

²A. Chambers and D. C. Jackson, *Philos. Mag.* **31**, 1357 (1975).

³C. T. Horng and R. W. Vook, *J. Vac. Sci. Technol.* **11**, 140 (1974).

⁴Y. C. Lee, H. Min, and P. A. Montano, *Surf. Sci.* **166**, 391 (1986).

⁵G. K. Wertheim and D. N. E. Buchanan, *Phys. Rev. B* **33**, 914 (1986).

⁶S. A. Chambers, H. W. Chen, I. Vitomirov, S. B. Anderson, and J. H. Weaver, *Phys. Rev. B* **33**, 8810 (1986).

⁷L. A. Bruce and H. Jaeger, *Philos. Mag.* **36**, 1331 (1977).

⁸W. F. Egelhoff, *Phys. Rev. B* **30**, 1052 (1984); *J. Vac. Sci. Technol. A* **2**, 350 (1984).

⁹E. Bauer and H. Poppa, *Thin Solid Films* **12**, 167 (1972); J. L. Moran-Lopez, G. Kerker, and K. H. Bennemann, *Surf. Sci.* **66**, 641 (1977).

¹⁰M. De Crescenzi and G. Chiarello, *J. Phys. C* **18**, 3598 (1985).

¹¹M. De Crescenzi, *J. Vac. Sci. Technol. A* **5**, 869 (1987); *Critical Reviews in Solid State and Materials Sciences* (Academic, New York, in press).

¹²M. De Crescenzi, M. Diociaiuti, L. Lozzi, P. Picozzi, and S. Santucci, *Phys. Rev. B* **35**, 5997 (1987).

¹³G. Apai, J. F. Hamilton, J. Stöhr, and A. Thompson, *Phys. Rev. Lett.* **43**, 165 (1979).

¹⁴Y. U. Idzerda, E. D. Williams, T. L. Einstein, and R. L. Park, *Surf. Sci.* **160**, 75 (1985).

¹⁵T. Tyliszczak and A. P. Hitchcock, *J. Vac. Sci. Technol. A* **4**, 1372 (1986).

¹⁶P. Roubin, D. Chandesris, G. Rossi, J. Lecante, M. C. Desjonqueres, and G. Treglia, *Phys. Rev. Lett.* **56**, 1272 (1986).

¹⁷M. C. Desjonqueres and G. Treglia, *Phys. Rev. B* **34**, 6662 (1986).

- ¹⁸M. Bader, A. Puschmann, C. Ocal, and J. Haase, *Phys. Rev. Lett.* **57**, 3273 (1986).
- ¹⁹F. Sette, C. T. Chen, J. E. Rowe, and P. H. Citrin, *Phys. Rev. Lett.* **59**, 311 (1987).
- ²⁰K. Baberschke, *Surf. Sci.* (to be published).
- ²¹L. Papagno and L. S. Caputi, *Surf. Sci.* **125**, 530 (1983); A. G. Nasiopoulos and J. Cazaux, *ibid.* **165**, 203 (1986).
- ²²J. Stöhr, in *Principles, Techniques and Applications of EXFAS, SEXAFS and XANES*, edited by R. Prins and D. C. Koningsberger (Wiley, New York, 1987).
- ²³M. De Crescenzi, A. P. Hitchcock, and T. Tylliszczak (unpublished).
- ²⁴T. Tylliszczak, A. P. Hitchcock, and M. De Crescenzi (unpublished).
- ²⁵J. G. Tobin, S. W. Robey, and D. A. Shirley, *Phys. Rev. B* **33**, 2270 (1986); J. G. Tobin, S. W. Robey, L. E. Klebanoff, and D. A. Shirley, *ibid.* **35**, 9056 (1987).
- ²⁶J. Lecante, Y. Ballu, and D. M. Newus, *Phys. Rev. Lett.* **38**, 36 (1977).
- ²⁷N. Avery, *Surf. Sci.* **111**, 358 (1981).
- ²⁸A. P. Hitchcock and C. H. Teng, *Surf. Sci.* **149**, 558 (1985).
- ²⁹M. De Crescenzi, L. Papagno, G. Chiarello, R. Scarmozzino, E. Colavita, R. Rosei, and S. Mobilio, *Solid State Commun.* **40**, 613 (1981).
- ³⁰L. Papagno, M. De Crescenzi, G. Chiarello, E. Colavita, R. Scarmozzino, L. S. Caputi, and R. Rosei, *Surf. Sci.* **117**, 525 (1982).
- ³¹B. K. Teo and P. A. Lee, *J. Am. Chem. Soc.* **101**, 2815 (1979).
- ³²W. E. Ekardt and D. B. Tran Thoai, *Solid State Commun.* **45**, 1083 (1983).
- ³³M. Fanfoni, S. Modesti, N. Motta, M. De Crescenzi, and R. Rosei, *Phys. Rev. B* **32**, 7826 (1985).
- ³⁴R. C. Albers, A. K. McMahan, and J. E. Muller, *Phys. Rev. B* **31**, 3435 (1985).
- ³⁵E. Chainet, M. De Crescenzi, and J. Derrien, *Phys. Rev. B* **31**, 7469 (1985).
- ³⁶D. B. Tran Thoai, A. Santoni, W. Ekardt, and J. Urban, *Solid State Commun.* **58**, 315 (1986).
- ³⁷F. Combet-Farnoux and A. P. Hitchcock, *Solid State Commun.* **64**, 961 (1987).
- ³⁸F. Jona, *J. Phys. C* **11**, 4271 (1978); P. R. Watson, F. R. Shepherd, D. C. Frost, and K. A. R. Mitchell, *Surf. Sci.* **72**, 562 (1978).
- ³⁹P. A. Lee, P. M. Citrin, P. Eisenberger, and B. E. Kincaid, *Rev. Mod. Phys.* **53**, 769 (1981).
- ⁴⁰E. Sevilano, H. Meuth, and J. J. Rehr, *Phys. Rev. B* **20**, 4908 (1979).
- ⁴¹Y. U. Idzerda, E. D. Williams, T. L. Einstein, and R. L. Park, *Phys. Rev. B* **36**, 5941 (1987).
- ⁴²R. B. Greegor and F. W. Lytle, *Phys. Rev. B* **20**, 4902 (1979).
- ⁴³W. Böhmer and P. Rabe, *J. Phys. C* **12**, 2465 (1979).
- ⁴⁴J. B. Pendry, *Low Energy Electron Diffraction* (Academic, London, 1974).
- ⁴⁵D. K. Saldin, *Surf. Sci.* (to be published).
- ⁴⁶Y. Ohno, *Phys. Rev. B* **36**, 7500 (1987).
- ⁴⁷F. P. Netzer and M. M. El Gomati, *Surf. Sci.* **124**, 26 (1983).
- ⁴⁸T. Tylliszczak and A. P. Hitchcock (unpublished).
- ⁴⁹C. S. Jayanthi, E. Tosatti, and L. Pietouero, *Phys. Rev. B* **31**, 3456 (1985).